A Curved Compliant Differential Mechanism With Neutral Stability

Mak, Robin; Nobaveh, Ali Amoozandeh; Radaelli, Giuseppe; Herder, Just L.

Important note
To cite this publication, please use the final published version (if applicable).
Please check the document version above.

Robin Mak[1]
Department of Precision and Microsystems
Engineering,
Delft University of Technology,
Delft 2628 CD, The Netherlands
e-mail: Robinmak_nl@hotmail.com

Ali Amoozandeh Nobaveh[1]
Department of Precision and Microsystems
Engineering,
Delft University of Technology,
Delft 2628 CD, The Netherlands
e-mail: A.AmoozandehNobaveh@tudelft.nl

Giuseppe Radaelli
Department of Precision and Microsystems
Engineering,
Delft University of Technology,
Delft 2628 CD, The Netherlands
e-mail: G.Radaelli@tudelft.nl

Just L. Herder
Department of Precision and Microsystems
Engineering,
Delft University of Technology,
Delft 2628 CD, The Netherlands
e-mail: J.L.Herder@tudelft.nl

A Curved Compliant Differential Mechanism With Neutral Stability

Differential mechanisms are remarkable mechanical elements that are widely utilized in various systems; nevertheless, conventional differential mechanisms are heavy and difficult to use in applications with limited design space. This paper presents a curved differential mechanism that utilizes a lightweight, compliant structure. This mechanism acquires its differential characteristic by having a high rotational stiffness when the mechanism is symmetrically actuated on two sides, while having a low rotational stiffness when actuated only on one side. To make the mechanism neutrally stable, the intrinsic elastic strain energy required for deformation of the compliant differential is compensated for by the reintroduction of potential energy, which is provided by two preloaded springs. The rotational stiffness of the one-sided actuation of the compliant differential mechanism around the neutral position is hypothesized to be adjustable by changing the preload of the springs. The stiffness can be positive, zero, or negative, indicating that the mechanism can be neutral or bistable. This hypothesis is investigated using a simulated model in Ansys Parametric Design Language (APDL) using optimized parameters to achieve the desired stiffness for the mechanism. The simulated model is validated using an experimental setup for both the one-sided and symmetrical actuation stages. The experimental results showed a high correlation with the simulation results. The mechanism with optimized dimensions and preload demonstrated neutral stability over a 16 deg range. Bistability was discovered for preloads greater than the optimized preload. At $\theta = 0$, a linear relationship was discovered between the spring preload and the rotational stiffness of the mechanism. Furthermore, an output/input kinematic performance of 0.97 was found for the simulated results and 0.95 for the experimental results. [DOI: 10.1115/1.4056867]

Keywords: compliant mechanisms, differential mechanism, neutral stability, zero stiffness, wearable devices

1 Introduction

The first recorded instance of a differential mechanism being used in a mechanism was over 2000 years ago in the Antikythera mechanism, which used differential gears [1]. The differential mechanism was used to determine the angle between the ecliptic positions of the Sun and Moon. Other uses of differential mechanisms in history are for the use as a compass around 250 AD by engineer Ma Jun [2], or by clockmaker Joseph Williamson in a clock mechanism. One of the most known uses for differential mechanisms is as an automobile differential, which was invented by Onésiphore Pecquer in 1827 [3]. In this long history of differential mechanisms, only conventional mechanisms using predominantly gears were found. Only one compliant differential mechanism by Valentijn was found [4]. He used a thin-walled warping beam to create differential behavior in his mechanism. The principle of using warping for rotational transmission is explained in Ref. [5].

Compliant mechanisms are mechanisms that use elastic deformation to accomplish something useful [6]. Traditionally, when designers needed movement within a mechanism, they only used rigid bodies connected with hinges and sliding joints. However, when you look at nature, much more flexibility in movement can be seen. Think of bee wings, elephant trunks, eels, seaweed, spines, and the blooming of flowers. Very compact mechanisms using this flexible behavior can be seen in nature. Compliant mechanisms have many advantages, such as significantly lower cost due to fewer parts and monolithic construction, increased precision due

to reduced wear and eliminated backlash, no need for lubrication, and generally a reduction in mass and size. However, compliant mechanisms also introduce some challenges, such as a more difficult simultaneous design process for motion and force behavior, fatigue life needs to be addressed, the motion is often more limited than traditional rigid-link mechanisms with no continuous rotation possible, there are higher stress concentrations, and most importantly, they require energy during movement due to elastic deformation [7].

A way to have the benefits of a compliant mechanism, but eliminate the energy stored during elastic deformation, is to make the mechanism neutrally stable [8–11]. This technique was also widely used in compliant flexural pivots to make them neutrally stable in a certain range of motion [12,13]. If the input and output energies of the mechanism are the same over a range of motion, the potential energy will be constant with the initial assumption that the system is isolated and conservative [10]. Several equivalent descriptions for this behavior exist, such as neutral stability, continuous equilibrium, constant potential energy, or zero stiffness [11]. A method to make a mechanism neutrally stable is to reintroduce energy into the energy stream between the input and output of the system [14].

There are multiple ways to store the potential energy in a system to compensate for the elastic strain energy. This could be done by creating prestresses in the material [11,15] or during the assembly process [16,17]. Prestressing is also possible by adding an external compensator, which can be another compliant element or a conventional element like a spring. An example of a mechanism that uses an external prestressed compensator is proposed by Herder [18], who added a rolling-link spring mechanism to a compliant laparoscopic grasper to eliminate stiffness in this compliant grasper. This idea was further developed by Stapel, who proposed preloaded compliant flexures to reduce the stiffness of the aforementioned compliant laparoscopic grasper [19]. Although the storage and
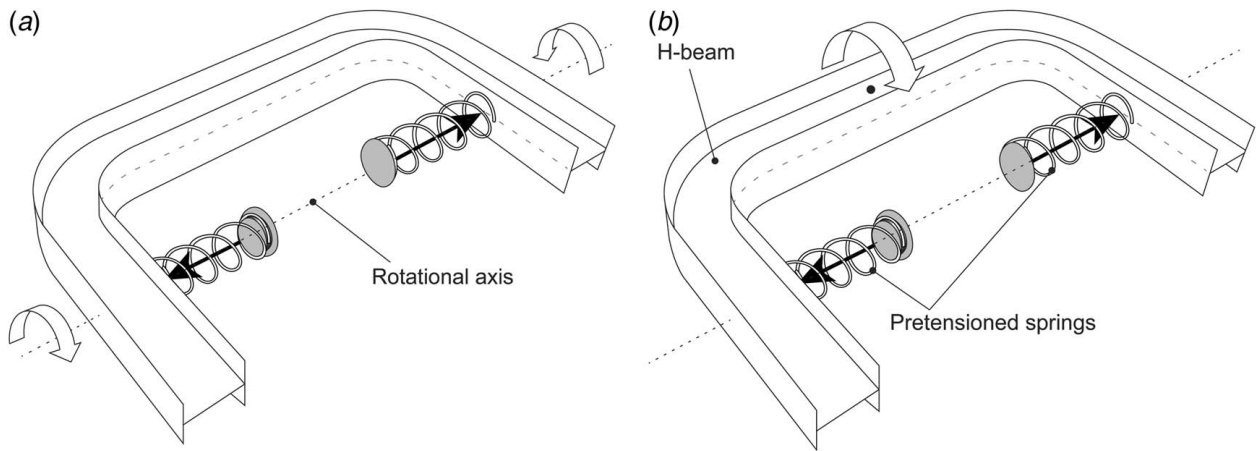
Fig. 1 A schematic view of the compliant differential mechanism. The dotted line indicates the rotational axis of the mechanism and the arrows show the rotation around each side of the mechanism and the middle output. The pretensioned springs are used to compensate the energy required for compliant mechanism's elastic deformation. (*a*) The one-sided input to output connection is with zero stiffness and energy free and (*b*) The symmetric drive from the middle to the side outputs has a very high stiffness.

reintroduction of potential energy have been widely exploited in the past to create compliant mechanisms with zero stiffness, no neutrally stable compliant differential mechanism has been reported.

The goal of this work is to demonstrate the use of a compliant differential mechanism in conjunction with a stiffness reduction technique by reintroducing energy to compensate for the potential elastic strain energy within the range of movement of the mechanism. Reintroduction of energy changes the stiffness of the mechanism from positive stiffness to zero stiffness or negative stiffness. The behavior of the mechanism is investigated and enhanced using simulations and optimization. The simulated results are validated using an experimental setup with a physical prototype. The experiments show a good match between anticipated and actual results in adjusting the stiffness and achieving high kinematic performance.

In Sec. 2, the working principle and intended application of the mechanism are explained. In Sec. 3, the details of the modeling together with the experimental setup are explained. In Sec. 4, the results of both the simulations and experimental setup are shown and discussed in Sec. 5. Finally, in Sec. 6, a conclusion is drawn from the results.

2 Working Principle

The compliant differential mechanism can be seen in Fig. 1. The mechanism works by having two pretensioned springs pushing outwards on the inside of the U-shaped open section thin-walled beam. While actuating the mechanism on one side, an opposite
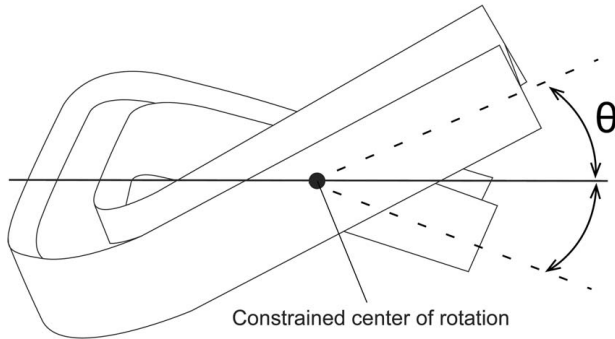

Fig. 2 A side view of the one-sided actuation, θ indicates the angular displacement of the input. The motion transferred to the output can also be seen on the other side of the mechanism.

rotation on the other side of the mechanism is generated. This one-sided actuation can be seen in Figs. 1(*a*) and 2. During this actuation, the springs are decompressed and transfer their potential energy into the energy required for the elastic deformation of the mechanism. The springs are constrained to be always aligned with the rotational axis of the mechanism, in this way, the springs only experience compression and decompression without any translation or bending in other directions. The transfer of energy causes the energy required to actuate the mechanism to be lower, which in turn lowers the rotational stiffness of the mechanism in one-sided actuation mode, while the symmetrical actuation mode still has a very high rotational stiffness. This latter actuation mode can be seen in Fig. 1(*b*). This mechanism has the interesting behavior of a differential mechanism.

The mechanism is hypothesized to work in a way in which the required elastic strain energy is compensated with a source of potential energy. When the mechanism is actuated on one side, the sides of the beam go out of plane and make skew lines, this causes the springs to decompress and go to a lower energy state. At the same time, the U-shaped beam is going to a higher energy state during elastic deformation. The sum of these two energies can be designed to be the constant. Due to the conservation of energy in an isolated and conservative mechanical system [10], the total potential elastic energy of all components would then be expected to look like Fig. 3, the dotted line is the potential spring energy of the two springs, the dashed line is the potential elastic strain energy of the mechanism. The total potential energy can be found by the summation of both the potential energy of the beam and the potential energy of the springs. This total energy is illustrated by the solid line, for which a constant level can be observed for a range of motion. This constant potential energy can be categorized as "neutral stability." The second derivative of the potential energy is the stiffness, so when the potential energy is constant, the stiffness and actuation force of the mechanism are both zero.

If the springs lose more energy than the energy required for the elastic deformation of the beam, a different behavior will be observed, which will create a peak in the potential energy with two minima on each side. This behavior would be classified as bistable, with two stable equilibrium points at the two local minima and an unstable equilibrium point at the peak of the potential energy. This unstable equilibrium indicates a negative stiffness when the potential energy is differentiated twice.

This would indicate that three different states can be achieved. A state with positive stiffness when no or insufficient energy compensation is used. A state with zero stiffness when the potential elastic strain energy is perfectly compensated. And lastly, a state with
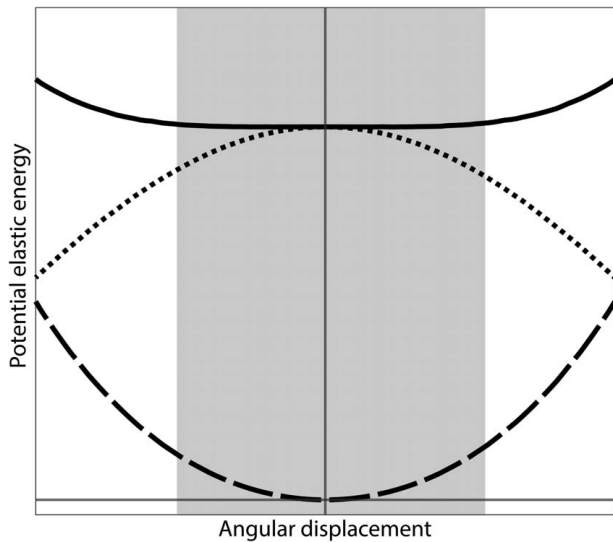
Fig. 3 The hypothesized total potential elastic energy (solid line) of the neutrally stable mechanism in its range of motion. This line is a summation of the energy of the beam (dashed line) during elastic deformation and the potential energy of the pretensioned springs (dotted line). The range of motion with a constant total potential energy is shown in gray.

negative stiffness occurs when the stored potential energy released is greater than the potential elastic strain energy required to actuate the mechanism. The released energy of the spring is a function of the initial preload, stiffness, and amount of decompression of the spring.

This behavior of varying the stiffness of the mechanism, specifically the zero stiffness state is further investigated and validated on a physical prototype.

The original design purpose of this compliant differential mechanism was for the use in a passive exoskeleton as a back support where the U-shaped beam is located around the waist, with the two sides connected to the legs and the middle part connected to the upperbody. During walking, you have alternating hip flexion on one side and hip extension on the other side. When bending there is hip flexion on both sides of the hip joint simultaneously. For this use case, it is required that the mechanism has low stiffness when walking and high stiffness when bending. This makes the users walking easy and energy free while this high stiffness provides bending support. These two cases are referred to in this paper as one-sided actuation and symmetrical actuation respectively. Such a mechanism can be labeled as a differential mechanism.

The mechanism is required to be around the human body but still have a rotational axis that aligns with the rotational axis of the human hip joint. Therefore, a U-shaped beam is chosen with constraints on the side of the human hip to create a rotation axis around these constraints. In this research, this application was chosen as the basis for all parameters, requirements, and optimized values. The parameters are therefore chosen on the basis of human sizes and can be changed to suit other applications.

3 Method

The mechanism consists of a thin-walled beam, with an H-shaped cross-section, which has two bends forming a U-shape geometry. The mechanism can be found in Figs. 1 and 4. A force is applied to the sides of the mechanism at points L and R using two springs. The aim is to research and analyze the neutral stability and bistability behavior of the mechanism and the changes in rotational stiffness due to the reintroduction of potential energy by changing spring parameters. Furthermore, the characteristics and performance of this mechanism as a compliant differential are
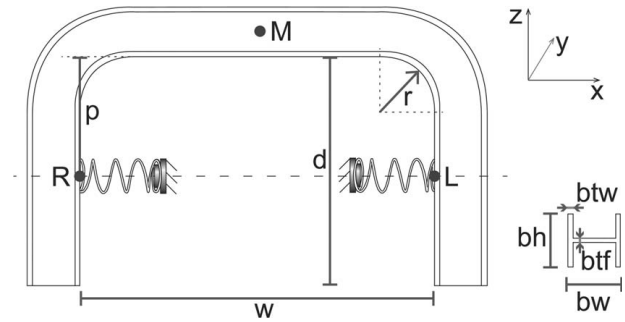

Fig. 4 The compliant differential mechanism investigated in this research is shown with its parameters. The location of the applied constraints and spring forces are also shown.

analyzed using simulations and experimental results for various initial spring preloads.

3.1 Requirements. The mechanism is subjected to the requirements which are set for the aforementioned case of a passive exoskeleton. For this case, the one-sided actuation is used for walking, and the symmetrical actuation is used as a support for bending. In this research, a linearly increasing moment for symmetrical actuation is set to reach 30 N m after 20 deg of angular displacement. For the one-sided actuation scenario, the maximum moment for the one-sided actuation should be lower than 5 N m with a range of motion of 50 deg, between −25 deg and 25 deg for each side. Furthermore, the mechanism should be as compact and lightweight as possible.

3.2 Geometry. The geometry of the mechanism can be found in Fig. 4. The cross-section of the beam was chosen to be H-shaped. This cross-section was chosen due to initial tests showing cross-sections with low torsional stiffness, high bending stiffness, and a high warping constant would perform better for the desired differential behavior.

The mechanism is constrained at three points, each constraining two degrees of freedom, thus, a total of six degrees of freedom are constrained in this monolithic mechanism, which makes it iso-constrained. The locations of the constraints are symmetric and located at points "R," "L," and "M" as seen in Fig. 4. The points "R" and "L" both constrain translation in the Y and Z directions and thus only move in the X direction while allowing rotation around all axes. Point "M" is constrained in translation in the Y and X directions and thus can move in the Z direction while allowing rotation around all axes. These constraints are the same for all loading scenarios. The preload force is applied to the points "R" and "L" in opposite directions in line with the X direction. This preload force is created by compressed linear springs.

3.3 Parameters. The parameters used for this mechanism are chosen for the passive exoskeleton case and stated in Table 1. Although the mechanism can be scaled to fit multiple design purposes, the parameters for this research are mainly based on anthropometric data and optimization using simulations in ANSYS, with a finite element solver. The width and depth of the mechanism have been obtained using anthropometric data from DINED [20] with the data set "Dutch adults, dined2004." w was obtained by taking a hip breadth of 400 mm plus two times 25 mm for the preloaded springs. p was obtained by taking half of the abdominal depth, which is chosen to align with the rotational axis of the hip joint. The hip breadth and abdominal depth were chosen around the 50 percentile of the age group of 20–60 years. These could be approximated because they will be used as input parameters for the optimization of the mechanism. For the radius of the two curves, R, early tests found that its contribution to the behavior of the beam was

Table 1 Parameters in this table are used for both modeling and experimental validation and are chosen based on an anthropometric data

Parameter	Symbol	Value
Inside width	w	450 mm
Inside depth	d	160 mm
	p	125 mm
Curve radius	r	25 mm
H profile height	bh	34 mm
H profile width	bw	34 mm
Web thickness	btw	0.8 mm
Flange thickness	btf	0.8 mm
Density	ρ	7880 kg m^{-3}
Poisson ratio	υ	0.275
Young's modulus	E	190 GPa
Free spring length	L_0	86.6 mm
Maximum spring force	F_n	102 N
Spring constant	c	1.49 N mm^{-1}

rather small. Therefore, it was removed from the scope of the research, and R was not varied in the optimization and has been chosen to follow the shape of the human body. bw and bh are the height and width of the H-profile cross-section. These were obtained using an optimization problem in MATLAB, which is further explained in Sec. 3.4.2. For this research, the thickness of the web and flanges have been chosen to be equal. The thickness has been found by manual optimization based on available stock material thicknesses for prototyping purposes. A thickness of 0.8 mm was found to be best suited for the chosen design parameters and requirements. The springs used to apply the preload to the mechanism are also chosen based on the required force F_n, free length L_n, and the highest possible spring constant c.

For the material AISI 301 or EN 1.4310, which is a hardened austenitic chromium-nickel stainless steel is used, with a Young's modulus E of around 190 GPa, and an ultimate tensile strength between 1300 and 1500 N mm^{-2}.

3.4 Modeling. For modeling the mechanism, APDL is used. The main advantage of this program is that the mechanism can be modeled using a scripting language and can be made as a parametric model. This ensures maximum control over the simulations and allows for simulating with different sets of parameters using MATLAB. By using an integration of ANSYS and MATLAB, it is possible to run the ANSYS model in an optimization problem to optimize the model for given input parameters and requirements of the mechanism.

The model is simulated in Ansys Parametric Design Language using finite element modeling (FEM). The model is fully parametric and is fully constructed in the APDL scripting language. For the simulation, a static analysis with a large deflection option is used. A shell model is selected to simulate the behavior of the beam. The shell is meshed using 8-nodal SHELL281 elements.

The constraints are as aforementioned and applied to the nodes at the locations of points "R," "L," and "M" on the shell. The preloading of the mechanism is performed by having two forces at points 'R' and 'L' in opposite directions. These forces simulate a linear spring in accordance with Hooke's law based on the U_x displacement of points "R" and "L."

3.4.1 Measurement. The modeled mechanism can be actuated in two different ways: one-sided actuation and symmetrical actuation. For the one-sided actuation scenario, a rotation is applied to a line of nodes on the left inside of the mechanism, this line of nodes spans 25 mm in both directions of the Z-axis with the point "R" in the middle. For the symmetrical actuation scenario, a line of nodes spanning a line in the Z direction at point "M" in the web. For both scenarios, the rotation is around the X-axis. To obtain the moment–angle and potential energy–angle curves, the required moment to actuate the mechanism to an angle in the range of motion has to be calculated. This is performed for both the one-sided actuation and symmetrical actuation scenarios. The one-sided actuation moment is calculated in the simulations by measuring the reaction forces at point "M." With the known distance from point "R" to "M," this accounts for a change in distance in the deformed state, and the moment around the rotational axis between points "R" and "L" can be calculated. For the symmetrical actuation scenario, a similar approach is taken, however for this scenario, the reaction forces on points "R" and "L" are measured and converted to a moment around point "M." The reaction forces can be exported directly from the simulations. To calculate the potential energy at a given angle, a cumulative trapezoidal numerical integration is used. This approximates the area under the moment–angle graph, which is the potential energy. The rotational stiffness of the mechanism is calculated by differentiating the moment–angle curve, the focus of this paper is mainly on the rotational stiffness at $\theta = 0$. The compliant differential mechanism has a difference in input angle and output angle, where the input angle is the actuated side of the mechanism and the output angle is the angle of the unactuated side, as can be seen in Fig. 2. In this research, the ratio between the input and output angles is defined as the kinematic performance. To calculate the kinematic performance of the compliant differential mechanism, the angle of both the actuated side and the unactuated side is measured. These angles are plotted against each other to find the correlation. From these data points, a linear regression is taken, for which the slope of this linear regression approximates the average kinematic performance over the complete range of motion.

3.4.2 Optimization. As discussed previously, the values of bw, bh and the initial preload to achieve neutral stability are found using optimization in MATLAB. This was performed by MATLAB running the ANSYS model with different sets of parameters. As the objective function, a weighted function of both the root-mean-square error (RMSE) of the one-sided actuation moment and a penalty function for the required symmetrical actuation moment is used. The RMSE is used to approximate zero stiffness at $\theta = 0$. The penalty function is used to constrain the lifting moment to fit the desired symmetrical actuation moment. Sequentially, the initial preload of the spring was optimized using the same RMSE to find the initial preload for which zero stiffness is achieved and thus neutral stability.

3.5 Experimental Validation

3.5.1 Physical Prototype. The physical prototype is constructed with a hardened stainless spring steel with the properties mentioned in Sect. 3.3. The thickness and properties of the material are in accordance with the simulated model. The material is laser cut with slits and wedges in the web and flanges to allow for alignment and fixation of the web and flanges. Although this gives a fairly rigid connection, it does not fully fixate the web and the flanges similar to the model. Therefore, spot welds are introduced to fixate the web and flanges.

3.5.2 Experimental Setup. The experimental setup in Fig. 5 consists of the mechanism attached to two axes on linear sliders which constrains the translation in the Y and Z directions for points 'R' and "L." To ensure that the constraint points are still allowed to freely rotate in all directions, a ball joint is used at the contact point between the axis and the inside flange of the mechanism. The preload force is applied to the mechanism using two springs which are attached to the two axes, this applies the force directly to the ball joint, and matches the simulated model. The constraint at point "M" is only in the Y direction, contrary to the simulated model which was also constrained in the X direction. However, this constraint was omitted for the experimental setup because the springs removed a degree of freedom, which constrained the mechanism in the X direction.

(a)

100 mm

Middle constraint

One-sided actuation
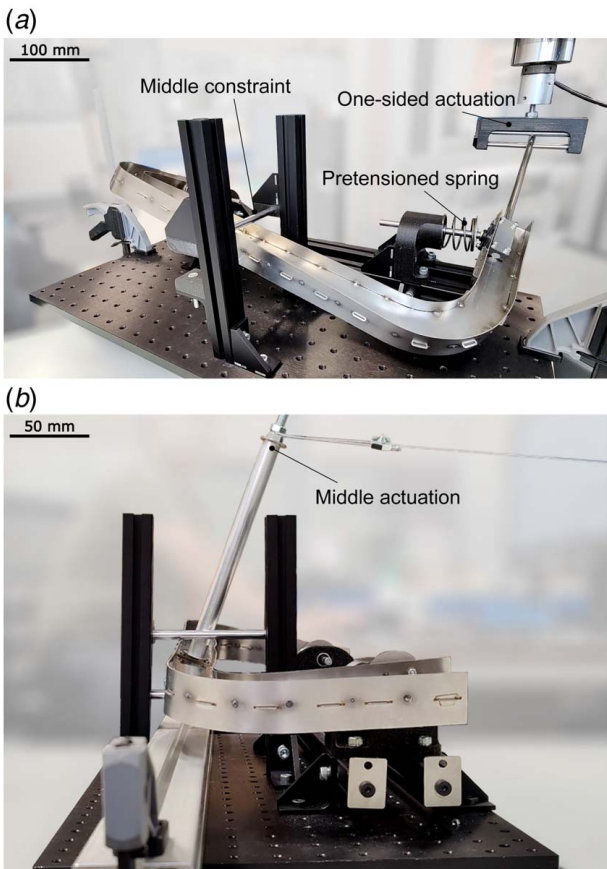
Pretensioned spring

(b)

50 mm

Middle actuation

Fig. 5 The experimental setup for validation of the simulated results for both the symmetrical actuation and one-sided actuation scenarios: (a) experimental setup for one-sided actuation and (b) experimental setup for symmetrical actuation

3.5.3 Measurement. To measure the moment–angle curve, a tensile testing machine is used to actuate one side of the mechanism using a rod attached to the flanges and the web on one side of the mechanism, as shown in Fig. 5(a). The universal testing machine operates at a speed of 200 mm min⁻¹. The measurement is performed by actuating one side of the mechanism to 25 deg and then to −25 deg before returning to 25 deg. The cycle is repeated twice for both sides of the mechanism to check for repeatability and to get more data points for smoother and more accurate results. The measured forces and displacements can be converted to a moment and angle with the known length and displacement of the actuation rod. The effect of the weight of the actuation rod is compensated for in the data processing. Due to Coulomb friction in the constraints, such as the ball joint and linear bearings, there is a hysteresis loop which centers around the predicted moment–angle curve, as can be seen in Fig. 6 in gray. The predicted true moment–angle curve can be subtracted from the hysteresis loop by averaging the higher and lower moments of the loop for each angle, this should be a close estimation if the mechanism is symmetrical and friction in both directions is assumed to be the same.

To measure the symmetrical actuation scenario, a rod is attached to the middle of the web at point 'M' a force is applied to this rod which causes a moment on the beam at the point of attachment. This force is applied using the tensile testing machine and a cable, as can be seen in Fig. 5(b). This force and the resulting displacement can be converted to a moment and an angle, respectively. The springs are also tested separately to see if their force–deflection behavior is similar to that of the modeled linear springs.

Finally, to calculate the kinematic performance, an additional rod is attached to the unactuated side of the mechanism to better visualize its angle. A camera and video analysis software are used to measure both the input and output angles to calculate the kinematic performance of the mechanism. This calculation was performed using the same method as the simulated results by finding the slope of the linear regression.

3.6 Experiments. In this research, four different scenarios are considered for the experiments. The first three scenarios are variations of the initial preload of the springs: no preload 0 N, an initial preload of 70 N which makes the mechanism neutrally stable, and an initial preload of 95 N where the mechanism shows bistable behavior. For the fourth scenario, a rotation is applied to point "M," the symmetrical actuation scenario. In this case, the preload effect is negligible and, therefore, is not considered in the tests.

4 Results

Figures 6(a)–6(c) show with the black line the resulting simulated moments for one-sided actuation for no initial preload, initial preload which led to neutral stability, and an initial preload which results in bistability. These moments are plotted against the angular displacement in degrees. The experimental results are shown with ◄ and ▷ symbols for left-side and right-side actuation, respectively. In light gray, the raw measured results are shown, these results show a hysteresis loop due to the friction in the experimental setup. As discussed in Sec. 3.5.3, friction in the experiment results is compensated for by averaging the moments.

Figures 6(d)–6(f) show the simulated potential energy in joules measured from the mechanism with the black line. Both of these cases are plotted against the angular displacement of one of the two actuated sides of the mechanism. The experimental results are shown with ◄ and ▷ symbols for left-side and right-side actuation, respectively. The potential energy is calculated from the sampled moment–angle curve. Hence, the friction in the results has already been compensated.

For the neutrally stable or zero stiffness scenarios, the results are shown in Figs. 6(b) and 6(e). The results in Fig. 6(b) show a near zero moment within a range of motion of 16 deg, between −8 deg and 8 deg. Also the results in Fig. 6(e) show a near constant potential elastic energy within the same range. The constant potential energy and a slope of zero can also indicate zero stiffness at $\theta = 0$.

For the bistable scenarios, the results are shown in Figs. 6(c) and 6(f). The results in Fig. 6(c) show a local minimum and a maximum at −10 deg and 10 deg, respectively. There are three locations where the moment is zero at −17 deg, 0 deg, and 17 deg, which are the equilibrium points. The results in Fig. 6(f) show the potential elastic energy with two local minima at −17 deg and 17 deg, which correspond to the equilibrium points in Fig. 6(c). Furthermore, the negative slope through $\theta = 0$ indicates negative stiffness. The experiments show the same behavior as the simulated results, but there is a slight difference. After the peaks the experimental results seem to have a steeper angle which indicates more stiffness, this can be observed in both the moment–angle curve and potential elastic energy–angle curve.

For the not preloaded scenarios, the results are shown in Figs. 6(a) and 6(f). The results in Fig. 6(a) show almost linear behavior going through the origin, which indicates an almost constant positive stiffness over the entire range of motion.

Figure 7 shows the moment for the symmetrical actuation scenario, the dashed line is the simulated moment for the symmetrical actuation scenario. These results show a linear relation with the angular displacement from 0 N m to the optimized value of 30 N m. The experimental results for the symmetrical actuation scenario are shown with the symbol. These experimental results show a deviation from the experimental results after 5 deg, after this point, a steeper slope can be observed which indicates a higher stiffness for the symmetrical actuation scenario.
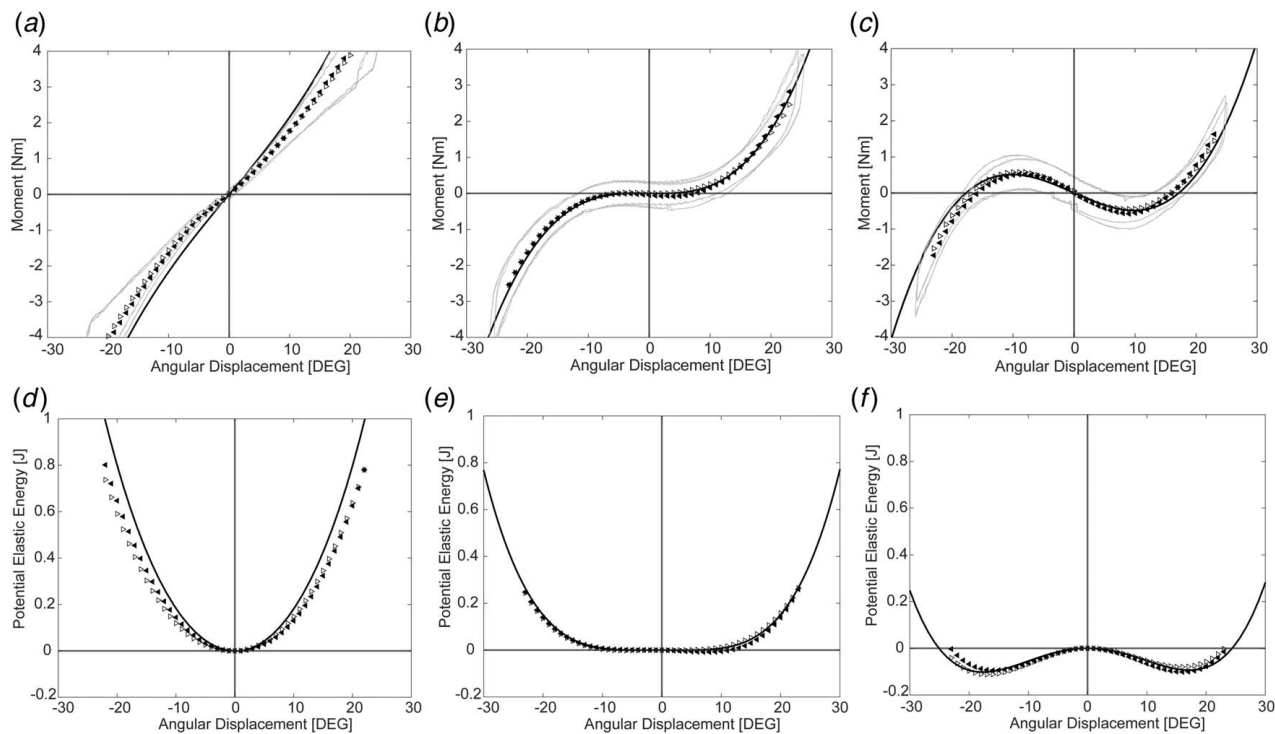
Fig. 6 The simulated (black) and the experimental (gray) results for the moment–angle and energy–angle of the mechanism in a one-sided actuation scenario with three different spring preloads. The ◄ and ▷ symbols show the friction compensated results for the left-side and right-side actuation, respectively. (*a*) Moment for 0 N preload. (*b*) Moment for 70 N preload. (*c*) Moment for 95 N preload. (*d*) Potential elastic energy for 0 N preload. (*e*) Potential elastic energy for 70 N preload and (*f*) Potential elastic energy for 95 N preload.

Figure 8 shows that within the tested initial preloads, the mechanism shows a linear relationship between the preload and the stiffness of the mechanism at $\theta = 0$. This linear relationship is shown in Eq. (1), where k_{ψ} is the rotational stiffness and F_p is the initial preload of the springs

$$k_{\psi} = -0.1673 F_p + 11.6153 \qquad (1)$$

This means that the initial preload is negatively correlated with the stiffness, and a higher initial preload results in a lower stiffness.
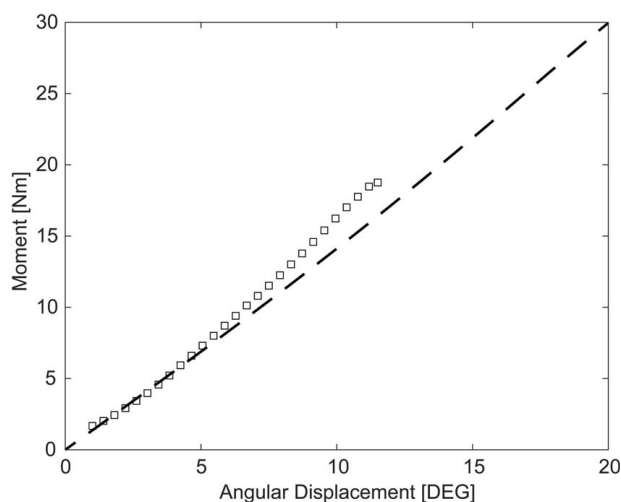
This behavior can also be observed for negative preloads, with a force pulling inward instead of pushing outward. For initial preloads at 70 N zero stiffness is observed, indicating neutral stability. While for initial preloads higher than 70 N negative stiffness is observed, which indicates bistability. The experimental results are shown with the calculated stiffness using the ■ symbol.

Figure 9 shows the kinematic performance of the different initial preloads from simulations. The dashed line shows a linear trend between the kinematic performance and the initial preload. The kinematic performance shows a linear trend between 0.96 and 0.98 for the simulations. The experimental result for the neurally

Fig. 7 The moment required for the symmetrical actuation case, for the simulated results (dashed line) and the experimental results. The experimental results are shown with the symbol.
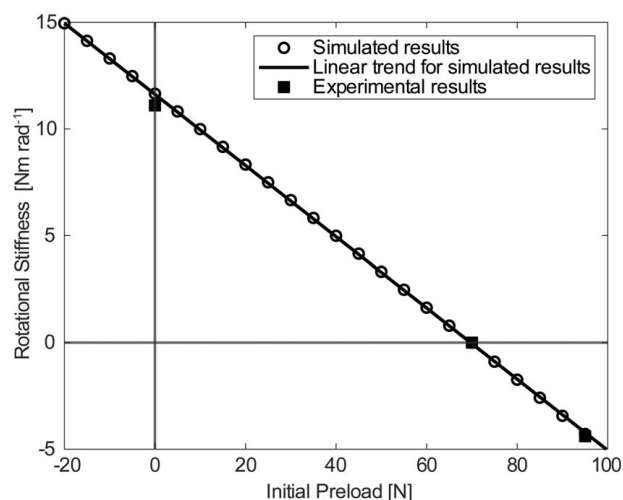
Fig. 8 The effect of the initial preload of the springs on the rotational stiffness of the mechanism
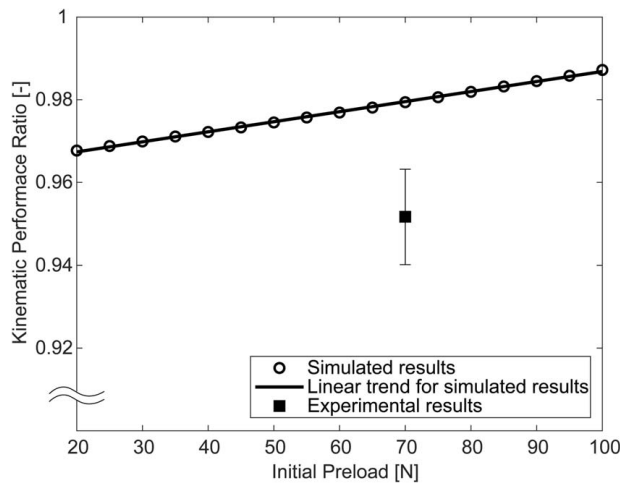
Fig. 9 Kinematic performance, the ratio between motion of the actuated side and the unactuated side, for different initial preloads are shown with a linear trend between them, the resulting ratio from the experiment is also shown

stable scenario which are shown with the ■ symbol in the same figure is 0.95 for a 70 N initial preload; the error bar indicates the 95% confidence range.

The linear approximation for the springs according to Hooke's law has been tested. The compression test has been performed on the springs used in the experimental setup. The springs showed the same linear behavior as the simulated springs, with the same expected spring stiffness of $1.49 \, \mathrm{N \, mm^{-1}}$.

5 Discussion

The expected behavior of neutral stability was found both in the simulations and experimental results for the optimized initial preload. This indicates that the current method, the reintroduction of potential energy, is an effective way to manipulate the stiffness. Furthermore, it is shown that by increasing the reintroduced potential energy, i.e., higher springs pretension, it is possible to achieve bistable behavior. This bistable behavior was observed in the simulated and experimental results.

The experimental results of the neutrally stable scenario almost perfectly match the simulated results. However, in bistable and non-preloaded scenarios, the experimental results show a small deviation from the simulated results. Furthermore, the results show consistency between cycles and sides of the mechanism. The small deviations could be due to the experimental setup, for example, the tool used to actuate the mechanism required a few millimeters of backlash to work properly, this is also the case for the fixation at point M. This backlash could cause a shift in the final processed results. This will be most pronounced in the not preloaded scenario due to the steeper slope. This backlash could be removed by creating better fixations.

Another discrepancy that could explain the differences between the simulations and the experimental results is the difference in exertion of the actuation. The simulated model is actuated only by applying an angular displacement, which differs from the experiments where it is applied by a linear displacement. This introduces forces into the system instead of only a pure moment. Furthermore, the effect of the difference in constraints between the ANSYS model and prototype seemed to be minimal but could be improved in future works.

Another source of difference between simulations and the experimental results can be due to the connection between the web and flanges, in the simulations, this is a uniform continuous rigid connection. However, in the experimental setup, a continuous connection was not feasible, and a connection using spot welds was used,

which gave the mechanism a rigid connection while minimally affecting the material properties at the connection. It is possible to use laser-welding to create a better fixation between the web and the flanges, this minimizes added material and only makes a relatively small heat affected zone. Another way to better match the results to the model is to model the connection between the web and the flanges in ANSYS.

For the symmetrical actuation scenario, the optimization to reach 30 N m at 20 deg was successful and resulted in constant rotational stiffness in the desired range of motion. However, in the experiments, a higher rotational stiffness was captured after 5 deg. This deviation could be caused by the difference in the exertion of the moment.

For the symmetrical actuation scenario, the full 20 deg of angular displacement could not be achieved due to buckling in the flanges, this buckling was observed after about 7 deg. The simulations also showed buckling, however, this only occurred at deformations higher than the 20 deg. Buckling at smaller deformations could be caused by the spot weld, which caused a nonuniform connection with the web, the spot welds also caused some slight imperfections in the flanges which could also cause an earlier buckling. Due to this buckling, the experiment was stopped after 12 deg of angular displacement.

The kinematic performance for the simulated results is around 2–3% lower than the ideal ratio of 100%. The measured experimental results show only a 2% difference with a 95% transfer of motion. This is a high percentage and is considered a good result. This deviation between the experiments and the simulated kinematic performance can be seen in Fig. 9. This could be explained by a few factors, which are sorted based on their effects. First, the friction in the experimental setup could cause losses in transferring motion from the input to the output side of the mechanism. This is believed to be the largest contributor to the discrepancy. Second, the minimum measurement unit for the angle using image processing was set to 1 deg. Finally, a camera was used to calculate the difference in angle between the actuated and unactuated arm; therefore, a difference in perspective or possible lens distortion can be another source of error during the measurements.

An important metric of this differential mechanism is the ratio between the rotational stiffness of the one-sided actuation (walking) and the symmetrical actuation (bending). This ratio for the range of motion of 20 deg is

$$\frac{\text{Symmetrical actuation}}{\text{One-sided actuation}} = \frac{30}{1.76} = 17 \qquad (2)$$

This is almost three times higher than the same ratio for the unpreloaded mechanism, for which this ratio is $\frac{30}{5.09} = 5.9$. This shows a significant increase in the difference in rotational stiffness by reintroducing energy to lower the overall rotational stiffness of the mechanism. The ratio could be even higher if the bistability of the mechanism was utilized; however, this bistability is not always desired. However, this bistability can be used to lower the overall required work to actuate the mechanism over a larger range.

When comparing the proposed compliant differential mechanism with the conventional differential mechanisms, the main advantages of the proposed design are the removal of backlash and friction, and the reduction in a number of parts and thus assembly time. The main disadvantage of stored elastic energy for compliant differential mechanisms has been alleviated for a range of 16 deg, conventional differential mechanisms do not have this disadvantage and only suffer from friction between the gears. This friction is relatively low, but it is hard to compare to the proposed design due to the scalability of this proof of concept. The second limitation of the proposed compliant differential mechanism is the limited range of motion, while conventional differential mechanisms have continuous rotations this is limited for the compliant design. This is however a limitation which is not a problem for all design purposes.

Now that the expected behavior has been found and verified, more future research can be done into this mechanism. The

design used for this proof of concept has been kept simple and uniform in order to find the behavior with as few variables as possible. In future research into the mechanism, a variation in the width and height of the beam could be investigated, for instance, the *bw* and *bh* of the beam could be optimized separately to see if the mechanism could be made more compact or have a wider range of motion with neutral stability and zero stiffness. Another interesting thing to look into is varying the thickness of the web and flanges as separate parameters, e.g., a lower thickness web could lower the stiffness of the mechanism while having less impact on the warping of the beam. Furthermore, from additional stress analysis that was outside the scope of this research, the two side sections around points "R" and "L" were found to be less important for the behavior of the mechanism and show much lower stresses than the straight back section. More narrow and compact dimensions could most likely be chosen for this area.

In addition to the dimensions, the cross-section could also be changed. While in initial testing a C-shaped and an I-shaped cross-sections seemed to perform worse than the H-shaped cross-section for the desired behavior, other sections could be further examined, especially if other parts of the mechanism are also altered. Cross-sections like open circular sections or T-profile which have not been looked into at all, could show different and possibly better behavior.

Another improvement is to change the source of potential energy storage in the mechanism. In the current version potential energy is stored in the external springs, but it can be replaced by prestresses in the mechanism itself. A similar approach to Lachenal [17] with pre-stressed flanges could be interesting to look into. Another approach would be to reduce the out-of-plane stiffness on the sides and store the potential energy in a fashion similar to that of the external springs in those two regions.

6 Conclusion

In this paper, a compliant differential mechanism with near zero stiffness is presented. A method to manipulate the rotational stiffness of the mechanism by reintroducing energy to compensate for the inherent strain energy of the compliant mechanism due to elastic deformation. The compensation energy is supplied by pretensioned springs. Three different initial preloads of these springs have been investigated to show the effect on the mechanism's behavior: no initial preload, initial preload which makes the mechanism neutrally stable, and finally, an initial preload which causes the mechanism to have negative stiffness and becomes bistable. It was found that for the optimized value of 70 N spring pretension a neutrally stable range of motion of 16 deg can be achieved. Furthermore, it is shown that the initial preloads of the spring had a linear relationship with the mechanism's rotational stiffness at its neutral position at $\theta = 0$. This was even the case for negative stiffnesses for initial preloads greater than 70 deg.

The initial requirements of the mechanisms were met. The maximum absolute moment between -25 deg and 25 deg for the one-sided actuation was 3.6 N m which is lower than the set requirement of 5 N m for walking, this was for the optimized initial preload of 70 N m. For symmetrical actuation, the mechanism was successfully optimized for the minimum required moment of 30 N m at 20 deg for bending. Due to the optimization of the mechanism, the dimensions of the mechanism were minimized while meeting the requirements.

The mechanism performed well as a compliant differential mechanism with high symmetrical stiffness and low stiffness when actuated from one side. The required moment after 20 deg of actuation was shown to be 17 times higher for the symmetrical actuation compared to the one-sided actuation. Furthermore, a high kinematic performance was observed for the one-sided actuation of more than

0.97 in the simulated results, with the experimental results showing only 2% lower.

It can be concluded that this compliant differential mechanism can be optimized to have a range of motion for which the potential energy can be near constant and that the stiffness outside of this range is also reduced significantly. This was validated using both simulations and experimental validation. Furthermore, the mechanism can be easily optimized to fit specified requirements for a chosen application. This application could be for the use in an exoskeleton design, for which the mechanism can be optimized for a specific user, or in other applications where having a monolithic, lightweight, and scalable mechanism is essential.

Conflict of Interest

There are no conflicts of interest.

Data Availability Statement

The datasets generated and supporting the findings of this article are obtainable from the corresponding author upon reasonable request.

References

[1] Wright, M. T., 2007, "The Antikythera Mechanism Reconsidered," Interdiscipl. Sci. Rev., **32**(1), pp. 27–43.
[2] Santander, M., 1992, "The Chinese South—Seeking Chariot: A Simple Mechanical Device for Visualizing Curvature and Parallel Transport," Am. J. Phys., pp. 782–787.
[3] Vantsevich, V. V., 2015, *Advanced Autonomous Vehicle Design for Severe Environments*, IOS Press, Amsterdam, The Netherlands.
[4] Valentijn, M. C., 2020, "Thin-Walled Warping Beams for Differential Mechanism Applications," Technical Report, Delft University of Technology.
[5] Amoozandeh Nobaveh, A., Herder, J. L., and Radaelli, G., 2023, "A compliant Continuously Variable Transmission (CVT)," Mech. Mach. Theory.
[6] Howell, L. L., 2001, *Compliant Mechanisms*, John Wiley & Sons, Hoboken, NJ.
[7] Howell, L. L., Magleby, S. P., and Olsen, B. M., 2013, *Handbook of Compliant Mechanisms*, Vol. 2, Wiley, Hoboken, NJ.
[8] Opdahl, P. G., Jensen, B. D., and Howell, L. L., 1998, "An Investigation Into Compliant Bistable Mechanisms," International Design Engineering Technical Conferences and Computers and Information in Engineering Conference, Vol. 80319, American Society of Mechanical Engineers, Paper No. V01BT01A046.
[9] Kok, S., Radaelli, G., Nobaveh, A. A., and Herder, J., 2021, "Neutrally Stable Transition of a Curved-Crease Planar Shell Structure," Extreme Mech. Lett., **49**, p. 101469.
[10] Gallego, J. A., and Herder, J., 2010, "Criteria for the Static Balancing of Compliant Mechanisms," Technical Report.
[11] Schenk, M., and Guest, S. D., 2014, "On Zero Stiffness," Proc. Inst. Mech. Eng. Part C.
[12] Morsch, F. M., and Herder, J. L., 2010, "Design of a Generic Zero Stiffness Compliant Joint," International Design Engineering Technical Conferences and Computers and Information in Engineering Conference, Montreal, Quebec, Canada, Aug. 15–18, Vol. 44106, pp. 427–435.
[13] Zhao, H., Zhao, C., Ren, S., and Bi, S., 2019, "Analysis and Evaluation of a Near-Zero Stiffness Rotational Flexural Pivot," Mech. Mach. Theory, **135**, pp. 115–129.
[14] Gallego, J. A., 2013, "Statically Balanced Compliant Mechanisms: Theory and Synthesis," Technical Report.
[15] Kebadze, E., Guest, S., and Pellegrino, S., 2004, "Bistable Prestressed Shell Structures," Int. J. Solids Struct., pp. 2801–2820.
[16] Daynes, S., and Weaver, P. M., 2013, "Stiffness Tailoring Using Prestress in Adaptive Composite Structures," Compos. Struct., **106**, pp. 282–287.
[17] Lachenal, X., Daynes, S., and Weaver, P. M., 2014, "A Non-linear Stiffness Composite Twisting I-Beam," J. Intell. Mater. Syst. Struct., pp. 744–754.
[18] Herder, J. L., 2000, "Statically Balanced Compliant Mechanisms (SBCM'S): An Example and Prospects," International Design Engineering Technical Conferences and Computers and Information in Engineering Conference, Baltimore, MD.
[19] Stapel, A., and Herder, J. L., 2004, "Feasibility Study of a Fully Compliant Statically Balanced Laparoscopic Grasper," International Design Engineering Technical Conferences and Computers and Information in Engineering Conference, Salt Lake City, UT.
[20] Huysmans, T., Goto, L., Molenbroek, J., and Goossens, R., 2020, "Dined mannequin," Tijdschr. Voor Hum. Factors, **45**, pp. 4–7.